CLIMATE

Observed trend in Earth energy imbalance may provide a constraint for low climate sensitivity models

Gunnar Myhre[1]*, Øivind Hodnebrog[1], Norman Loeb[2], Piers M. Forster[3]

Climate forcings by greenhouse gases and aerosols cause an imbalance at the top of the atmosphere between the net incoming solar radiation and outgoing longwave radiation from Earth. This Earth energy imbalance has strengthened over the period 2001 to 2023 with satellite data. Here, we show that low climate sensitivity models fail to reproduce the trend in Earth energy imbalance, particularly in the individual longwave and shortwave contributions to the imbalance trend. The inability to produce a strong positive shortwave and strong negative longwave Earth energy imbalance trend is found to be a robust feature in the low climate sensitivity models, especially for models with a climate sensitivity below 2.5 kelvin. The negative longwave contribution to Earth energy imbalance is driven by surface temperature increases and is therefore most pronounced in high climate sensitivity models, whereas the shortwave contribution is generally positive and amplified by greater surface warming.

A long-standing research question in climate science is how sensitive the climate is to increases in greenhouse gases (GHGs) (*1*–*3*). This climate sensitivity is taken as the surface temperature rise for a doubling of the CO_2 concentration (*4*, *5*). In the latest Intergovernmental Panel on Climate Change (IPCC) report, the best estimate of the equilibrium climate sensitivity (ECS) was assessed as 3°C, with a likely range from 2.5° to 4°C and a very likely range from 2° to 5°C (*4*). How clouds change in a warmer world is the main cause of the uncertainty in the climate sensitivity (*4*, *5*), with divergent results from observational studies (*6*–*9*). The recent warming over the first one to two decades of this century has been used as arguments for low climate sensitivity models being most realistic, in particular how feedback processes are represented for the recent warming trend (*10*, *11*). However, the pattern of observed sea-surface warming in the Pacific may have biased some of these findings (*12*).

The past decades have seen a continued increase in GHGs (*4*) combined with a reversal of the aerosol effect (*13*). A reduction in the cooling effect of aerosols has thus a warming effect, and the total effective radiative forcing has been accelerating over the past decades (*14*). The Earth energy imbalance (EEI) is increasing (*15*, *16*) and will likely give an accelerated warming over the coming years (*17*). Hodnebrog *et al.* (*16*) showed that climate models forced with observed sea-surface temperatures (SSTs) reproduce the satellite-retrieved strengthening in EEI from the Clouds and the Earth's Radiant Energy System (CERES), but all models have a weaker trend than the observed trend. Schmidt *et al.* (*18*) showed that the EEI trend, split into longwave (LW) and shortwave (SW) trends, differed markedly between the CERES satellite and in different configurations of a climate model. Here we use a large set of coupled climate models from the Coupled Model Intercomparison Project Phase 6 (CMIP6) (*19*) to illustrate that low climate sensitivity models have an EEI trend behavior that is inconsistent with the satellite-derived EEI trend.

Trend in EEI

Figure 1 shows the EEI over the period with CERES satellite data and compared with coupled climate model simulations from CMIP6. The model simulations are a combination of the historical simulation until 2014 combined with a SSP5-8.5 scenario from 2015 onward. The SSP5-8.5 scenario includes reductions in aerosols combined with a strong increase in GHG concentrations. The CERES data show a stronger trend in EEI than the multimodel CMIP6 mean and higher EEI in 2023 than any of the CMIP6 models. However, for individual CMIP6 models and ensembles, EEI is comparable to or higher at other periods than the CERES value in 2023. Interannual variability in EEI is clearly shown for the CERES data and the climate models. In simulations with observed SST, the interannual variability in the CERES data is largely reproduced by the climate models (*16*).

The strengthened EEI from CERES is further supported by an accelerated trend in the ocean heat content (OHC) (*14*, *20*–*22*). Discrepancies exist in the degree of acceleration among various OHC datasets, with best agreement between CERES and OHC datasets having better ocean coverage and filling in data in data-sparse regions (*23*).

Relationship of LW and SW EEI trend

To illustrate climate model differences and robustness between models, we use idealized CMIP6 experiments. In Fig. 2, the EEI is shown for a range of models for the experiment with a 1%/year increase in CO_2 concentrations (named 1pctCO2). All models show an increasing net EEI (Fig. 2A) but with a much larger model diversity when net EEI is split into LW (Fig. 2B) and SW EEI (Fig. 2C). LW and SW EEI are positive when reducing outgoing radiation at the top of the atmosphere, typically caused by an increase in absorption by GHGs (both anthropogenic and as climate feedback). An increase in surface temperature causes an increase in outgoing LW radiation and thus a negative LW EEI. The majority of models have a negative LW EEI after some years because the increase in surface temperature and more outgoing LW radiation overwhelm the positive effect from the increase in CO_2. However, several models have a positive or very weak LW EEI even after more than 100 years. With one exception, the models have a positive SW EEI mostly throughout the time period of increase in CO_2 caused by less snow and ice (*24*) and contributions from water vapor absorption (*25*) and clouds for several models (see discussions in next sections). Figure 2D shows the trend in LW EEI versus SW EEI for the CMIP6 models, with uncertainties reflecting variation among four 23-year periods over the model simulations. Consistent with Schmidt *et al.* (*18*), we find a robust linear relationship in the LW and SW EEI trends among model members and a marked spread in the trends. Periods of 23 years are selected to match the length of data available from CERES.

Linking trends in EEI with climate sensitivity

Figure 3A shows the 1pctCO2 experiment and the abrupt quadrupling of CO_2 (abrupt-4xCO2) experiment, with colors reflecting the ECS. The LW and SW EEI trends are calculated as a mean of four 23-year trends and ECS from regressions using the abrupt-4xCO2 experiment over 150 years (*26*) and thus consistent with ECS values derived elsewhere (*4*, *27*). The 1pctCO2 and abrupt-4xCO2 experiments show different trend relationships for LW and SW EEI, with the former having a weaker LW negative trend gradient as a sustained increase in CO_2 contributes to LW EEI imbalance. The shading in Fig. 3A shows that the net EEI is generally increasing in the 1pctCO2 experiment and decreasing in the abrupt-4xCO2 experiment. Figure 3A also includes atmosphere-only simulations with observed SST fields from 2001 to

[1]CICERO Center for International Climate Research, Oslo, Norway. [2]NASA Langley Research Center, Hampton, VA, USA. [3]Priestley Centre for Climate Futures, University of Leeds, Leeds, UK. *Corresponding author. Email: gunnar.myhre@cicero.oslo.no

2019 from Hodnebrog *et al.* (*16*). Atmosphere-only simulations in which climate drivers (GHGs and aerosols) have been kept constant for the period 2001 to 2019 align with the abrupt-4xCO2 experiment, and atmosphere-only simulations with an increase in GHGs (but constant aerosols) over the 2001 to 2019 period show LW and SW trends similar to those of the 1pctCO2 experiment. Notably, the low climate sensitivity models have much weaker changes in LW and SW EEI trends than the other models. In particular, the models with ECS below 2.5 K all show very weak LW and SW EEI trends. For models with an ECS of 4 K or higher, there is little alignment with the LW and SW EEI trends, and the models are widely spread along the regression line. Nevertheless, it is notable that none of these models show very weak LW and SW EEI trends.

In Fig. 3B, the CERES satellite LW and SW EEI trend is shown together with the CMIP6 intramodel ensemble mean LW and SW EEI trend for the period 2001 to 2023. CMIP6 simulations are from a combination of the historical simulation until 2014 and the SSP5-8.5 scenario from 2015. Results are very similar for other scenarios with aerosol reductions (e.g., SSP2-4.5). Additionally, atmosphere-only simulations with changes in GHG and aerosols from Hodnebrog *et al.* (*16*) are included in Fig. 3B; note that these are for the period 2001 to 2019. The number of ensemble members for each model is quite variable (table S1). Figure 3C shows results for all ensemble members included in this study. Figure 3, B and C, show systematic weak LW and SW EEI trends from low climate sensitivity models, consistent with Fig. 3A. Note that the relationship between climate sensitivity and net EEI trends shows no systematic pattern, and various intramodel ensemble members exhibit a wide range in the net EEI trend (fig. S1). All models with climate sensitivity below 2.5 K have very weak LW and SW EEI trends. It is worth mentioning some of the EEI trends of lighter colors in Fig. 3, B and C. FGOALS-f3-L has a LW EEI trend similar to that of CERES and a SW EEI trend 0.2 W m^{-2}/decade weaker than that of CERES, but this model has a climate sensitivity of 3.0 K (Fig. 3B). In Fig. 3C, one ensemble member out of 50 for MIROC6 has a SW EEI trend above 0.4 W m^{-2}/decade. MIROC6 has a climate sensitivity of 2.6 K. GISS-E2-2-G is among the very low climate sensitivity models, with an ECS of 2.4 K, and has one out of five ensemble members with a SW EEI trend above 0.4 W m^{-2}/decade (0.41) but with a near-zero LW EEI. The atmosphere-only simulations in Fig. 3B are closer to CERES LW and SW EEI trends than the fully coupled simulations of the same model. This can be illustrated by HadGEM3, which shows slightly weaker trends than CERES where observed SST is used, and much stronger trends in the coupled simulations. Similarly, NorESM2

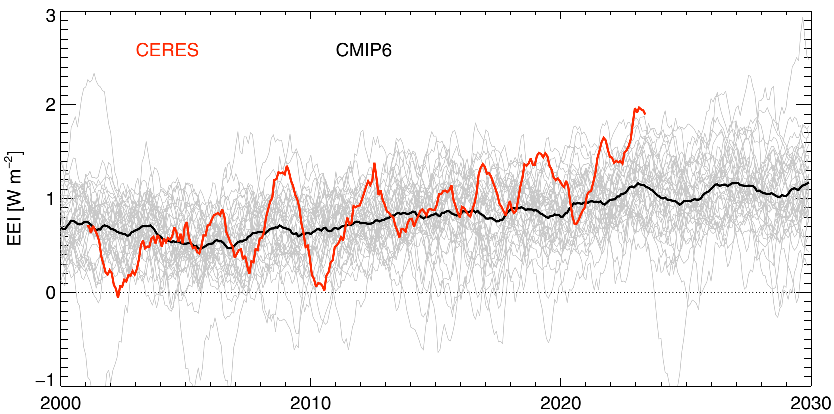

Fig. 1. Trend in EEI in CERES and CMIP6 models. The CERES data are shown from 2001 to 2023. The CMIP6 data are shown from 2000 to 2030. All EEI are given as 12-month running means. CMIP6 model mean is shown by a thick black line and individual models are shown in thin gray lines. Only one ensemble member for each of the models is shown.

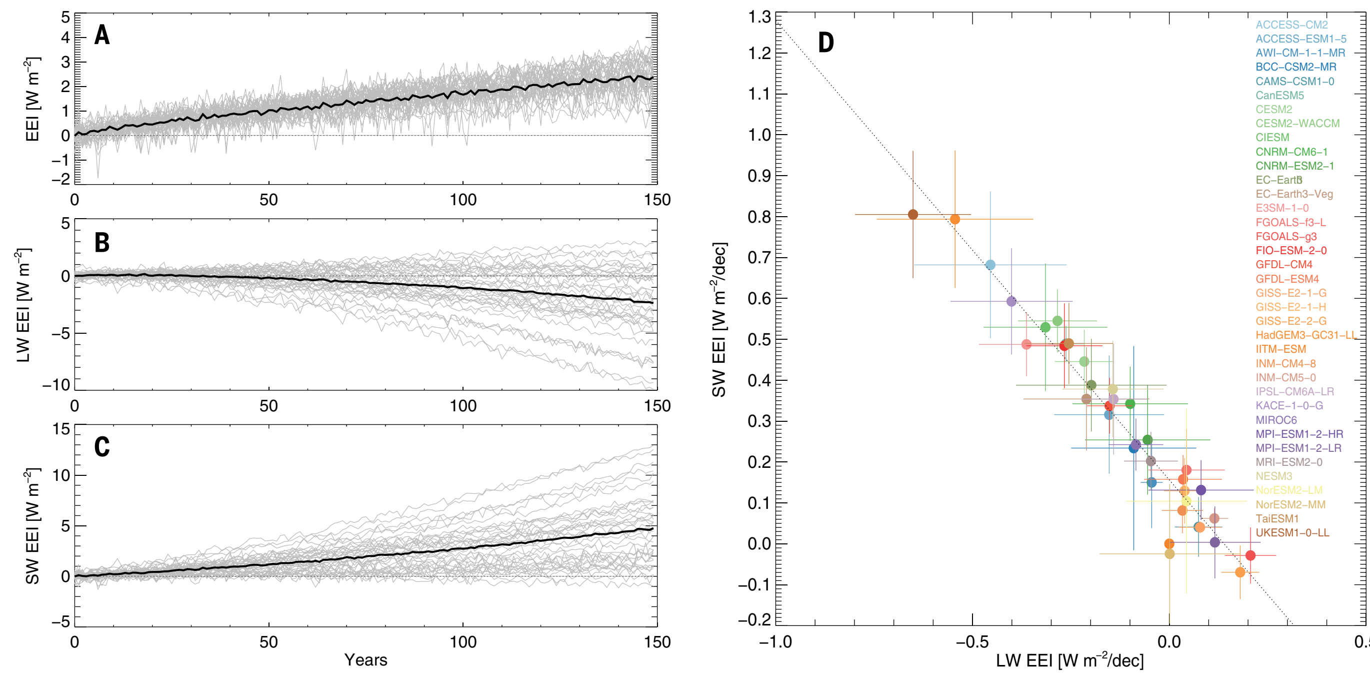

Fig. 2. EEI in CMIP6 models of 1%/year increase in CO$_2$ (1pctCO2). Net EEI (**A**), LW EEI (**B**), SW EEI (**C**), and SW EEI versus LW EEI trends where trends are derived from four 23-year intervals (**D**). Uncertainty ranges shown in (D) represent the standard deviation among the four 23-year intervals.

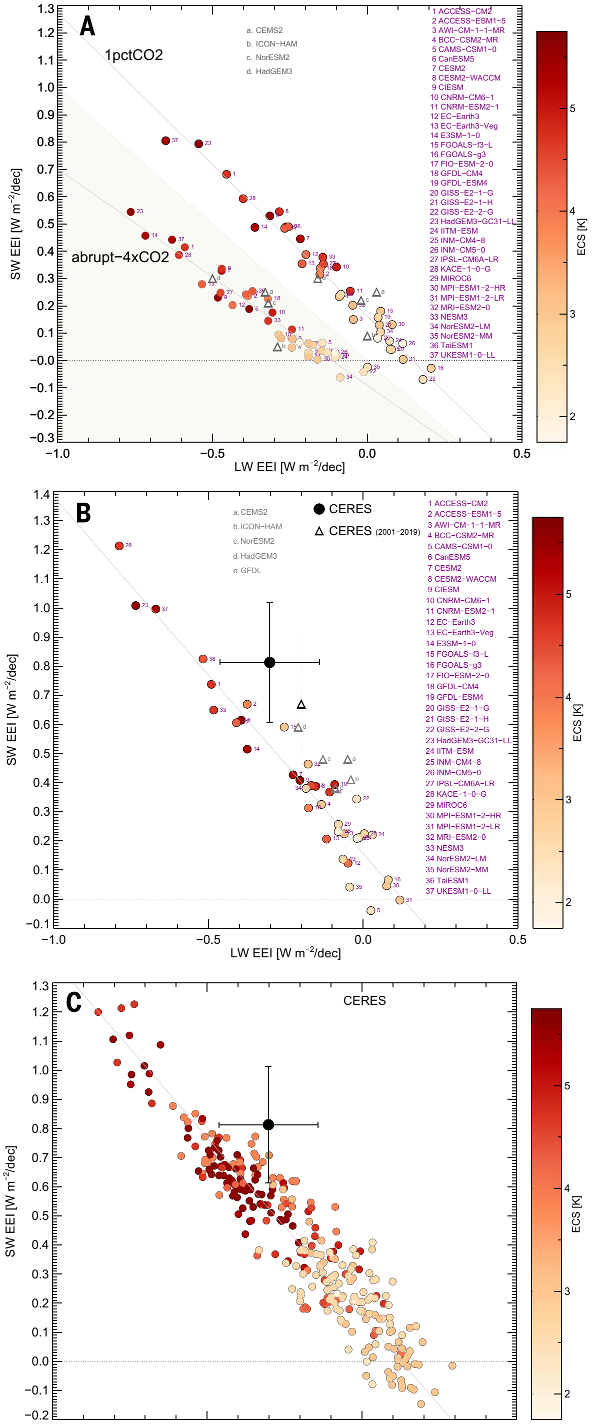

Fig. 3. SW EEI versus LW EEI trends and their relation to climate sensitivity in CMIP6 models. Primary ensemble member from each CMIP6 model for the abupt-4xCO2 and 1pctCO2 experiments with results from Hodnebrog *et al.* (*16*) on all driver constants (following abupt-4xCO2) and only GHG changes included (following 1pctCO2) (**A**); CERES and ensemble mean from each CMIP6 models (historical+SSP5-8.5) for 2001 to 2023 with results from Hodnebrog *et al.* (*16*) shown in gray colors for the period 2001 to 2019 (see further description in supplementary text) (**B**); and CERES and all individual ensemble members from CMIP6 models for 2001 to 2023 (**C**). The range of ECS in the CMIP6 models is from 1.9 to 5.6 K. In (A), the 1pctCO2 simulations have thicker lines around the circles than the abrupt-4xCO2 simulations. Yellow-gray shaded area in (A) shows where net EEI trend is negative. Lines around the CERES trends are 90% confidence intervals.

aligns better with CERES data when using observed SST simulations, showing stronger LW and SW EEI trends than in fully coupled simulations. However, differences with CERES are also evident among model simulations using observed SSTs, indicating that both the atmospheric and ocean components of the climate models contribute to differences in the LW and SW EEI trends.

Clear-sky LW and SW EEI trends show similar patterns to all-sky trends, with strong negative LW EEI trends for high climate sensitivity models and positive SW EEI trends in idealized CMIP6 experiments (fig. S2). The largest difference between the clear-sky and all-sky results are for SW EEI trends (Fig. 3A and fig. S2).

EEI trends and surface warming

The surface temperature warming differs substantially between the CMIP6 models, and Fig. 4 (and fig. S3 and fig. S4) investigates whether this alters the relationships shown in Fig. 3. The most notable result is that the CERES data show a higher SW EEI trend per degree warming than any of the CMIP6 models, and only the models with a strong negative LW EEI trend per degree warming are close to CERES (Fig. 4). The low climate sensitivity models have consistently much weaker LW and SW EEI trends per degree warming than the CERES data.

Discussion

The analysis above relates to models' long-term climate sensitivity estimated from abrupt 4xCO2 experiments. This can differ from their effective climate sensitivity, estimated from changes over the recent historical period. Previous studies find that climate models are unable to capture the recent pattern of East Pacific warming observed (*28*), and this is associated with reduced effective feedbacks and reduced effective climate sensitivity (*12*). Hodnebrog *et al.* (*16*) find that applying SST patterns to models improves EEI trends across models. When comparing the observed SST simulations (triangles) to their coupled modeled counterparts (circles) in Fig. 3B, low-sensitivity models such as NorESM exhibit relatively modest differences in the EEI trends and remain well below the CERES trend even with the observed SST pattern applied. Hence the particular observed SST pattern is unlikely to play a large role for the low climate sensitivity models, substantially underestimating the LW EEI and SW EEI trends compared to CERES.

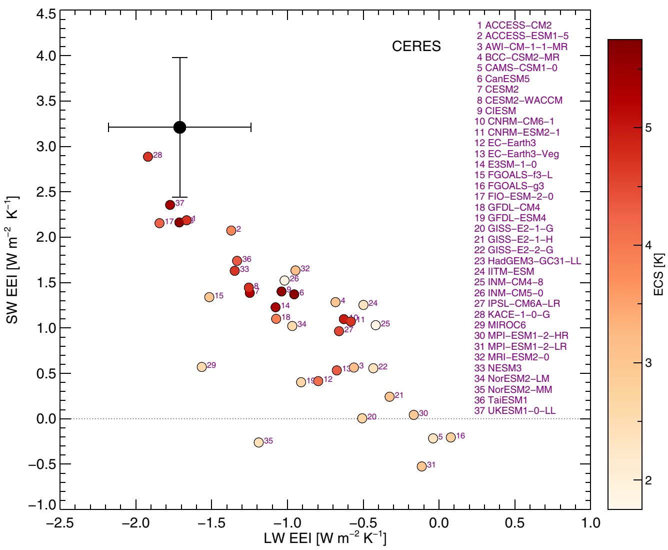

Fig. 4. SW EEI per degree warming trends versus LW EEI trends per degree warming in CMIP6 models and CERES satellite data. Colors show climate sensitivity of each CMIP6 model. Temperatures for the CERES data are taken from GISTEMP (*31*). Lines around the CERES trends are 90% confidence intervals.

Climate models consistently show a robust feature of a relationship between LW EEI and SW EEI trends, which varies depending on climate drivers involved in the simulations (Fig. 3, A and B). This relationship is also evident under clear-sky conditions (see fig. S2), where the positive SW EEI trend often is modest and driven by reduced surface albedo from less snow and ice in addition to contributions from SW absorption by water vapor. The negative LW EEI trend is driven by surface temperature increase and moderated if GHGs are increasing during the simulations. Cloud changes further amplify the clear-sky relationship between LW EEI and SW EEI trends. Figure S5 shows previously derived SW and LW cloud feedbacks (*27*) that exhibit a similar shape of relationship to that of LW EEI and SW EEI trends but slightly different gradient. Notably, SW cloud feedback demonstrates greater model diversity than LW cloud feedback, although the latter also shows substantial variability. A negative correlation between LW and SW cloud feedbacks can be expected as a result of the opposing warming and cooling effect of clouds on the climate system (*29*).

We show, using a large set of climate models, that trend in net EEI has no clear relationship to climate sensitivity. Consequently, we argue that the trends in net EEI and surface warming trend over the first two decades of this century provide little constraint on climate sensitivity. However, we present robust findings for trends in LW and SW EEI. These trends, and their relationship to climate sensitivity, are more physically based than the net EEI trend. The model distribution of EEI trends compared to CERES is shown in fig. S6. All models, given as the 99.999% level of the distribution, with an ECS of 2.93 K or below, are outside the CERES range. The models have a positive aerosol radiative forcing trend similar to that observed, around 0.16 W m^{-2} per decade (*16*, *30*). This would need to be underestimated by at least 50% to make the SW EEI trend from models with an ECS of 2.5 K match the CERES range, making such a low ECS unlikely.

REFERENCES AND NOTES

1. R. Knutti, M. A. A. Rugenstein, G. C. Hegerl, *Nat. Geosci.* **10**, 727–736 (2017).
2. J. Hansen *et al.*, *Science* **213**, 957–966 (1981).
3. G. H. Roe, M. B. Baker, *Science* **318**, 629–632 (2007).
4. P. Forster *et al.*, in *Climate Change 2021: The Physical Science Basis. Contribution of Working Group I to the Sixth Assessment Report of the Intergovernmental Panel on Climate Change,* V. Masson-Delmotte *et al.*, Eds. (Cambridge Univ. Press, 2021).
5. S. C. Sherwood *et al.*, *Rev. Geophys.* **58**, RG000678 (2020).
6. P. Ceppi, P. Nowack, *Proc. Natl. Acad. Sci. U.S.A.* **118**, e2026290118 (2021).
7. G. V. Cesana *et al.*, *Commun. Earth Environ.* **5**, 181 (2024).
8. I. Tan, T. Storelvmo, M. D. Zelinka, *Science* **352**, 224–227 (2016).
9. R. Vogel *et al.*, *Nature* **612**, 696–700 (2022).
10. A. Modak, T. Mauritsen, *Geophys. Res. Lett.* **48**, e2020GL091779 (2021).
11. D. Olonscheck, M. Rugenstein, *Geophys. Res. Lett.* **51**, e2023GL106909 (2024).
12. K. C. Armour *et al.*, *Proc. Natl. Acad. Sci. U.S.A.* **121**, e2312093121 (2024).
13. J. Quaas *et al.*, *Atmos. Chem. Phys.* **22**, 12221–12239 (2022).
14. P. M. Forster *et al.*, *Earth Syst. Sci. Data* **15**, 2295–2327 (2023).
15. N. G. Loeb *et al.*, *Geophys. Res. Lett.* **48**, e2021GL093047 (2021).
16. Ø. Hodnebrog *et al.*, *Commun. Earth Environ.* **5**, 166 (2024).
17. J. E. Hansen *et al.*, *Oxford Open Climate Change* **3**, kgad008 (2023).
18. G. A. Schmidt *et al.*, *Front. Clim.* **5**, 1202161 (2023).
19. V. Eyring *et al.*, *Geosci. Model Dev.* **9**, 1937–1958 (2016).
20. Z. Li, M. H. England, S. Groeskamp, *Nat. Commun.* **14**, 6888 (2023).
21. A. Minière, K. von Schuckmann, J.-B. Sallée, L. Vogt, *Sci. Rep.* **13**, 22975 (2023).
22. K. von Schuckmann *et al.*, *Earth Syst. Sci. Data* **15**, 1675–1709 (2023).
23. N. G. Loeb *et al.*, *Surv. Geophys.* **45**, 1757–1783 (2024).
24. A. Duspayev, M. G. Flanner, A. Riihelä, *Geophys. Res. Lett.* **51**, e2024GL109608 (2024).
25. A. Donohoe, K. C. Armour, A. G. Pendergrass, D. S. Battisti, *Proc. Natl. Acad. Sci. U.S.A.* **111**, 16700–16705 (2014).
26. J. M. Gregory *et al.*, *Geophys. Res. Lett.* **31**, L03205 (2004).
27. M. D. Zelinka *et al.*, *Geophys. Res. Lett.* **47**, e2019GL085782 (2020).
28. M. Rugenstein *et al.*, *Geophys. Res. Lett.* **50**, e2023GL105488 (2023).
29. V. Ramanathan *et al.*, *Science* **243**, 57–63 (1989).
30. P. M. Forster *et al.*, *Earth Syst. Sci. Data* **16**, 2625–2658 (2024).
31. N. J. L. Lenssen *et al.*, *J. Geophys. Res. Atmos.* **124**, 6307–6326 (2019).
32. G. Myhre, Fig3b,c [Data set], Zenodo. https://doi.org/10.5281/zenodo.15087491.

ACKNOWLEDGMENTS

Funding: The European Union's Horizon 2020 research and innovation program under grant agreement 820829 (CONSTRAIN) (G.M., Ø.H., P.M.F.) and project grants no. 325270 by the Norwegian Research Council (G.M., Ø.H.). **Author contributions:** Conceptualization: G.M. Methodology: G.M., Ø.H., N.L., P.M.F. Investigation: G.M., Ø.H., N.L., P.M.F. Formal analysis: G.M. Visualization: G.M. Validation: G.M., Ø.H., N.L., P.M.F. Writing – original draft: G.M. Writing – review & editing: G.M., Ø.H., N.L., P.M.F. **Competing interests:** The authors declare that they have no competing interests. **Data and materials availability:** CMIP6 model data used in this study are freely available from the CMIP6 repository on the Earth System Grid Federation nodes (https://esgf-node.llnl.gov/search/cmip6/, World Climate Research Programme, 2020). Derived LW and SW EEI from CMIP6 data presented in Fig. 3, B and C, are available at Zenodo (*32*). CERES EBAF-TOA Edition4.2 data were obtained from the NASA Langley Research Centre CERES ordering tool at https://ceres.larc.nasa.gov/data/. Global temperatures are from GISTEMP Team, 2024: GISS Surface Temperature Analysis (GISTEMP), version 4, NASA Goddard Institute for Space Studies, dataset accessed 2024-07-05 at https://data.giss.nasa.gov/gistemp/. Results for observed SST simulations are from Hodnebrog *et al.* (*16*).

SUPPLEMENTARY MATERIALS

science.org/doi/10.1126/science.adt0647
Materials and Methods; Supplementary Text; Figs. S1 to S6; Tables S1 and S2; References (*33*, *34*)

Submitted 12 September 2024; accepted 7 April 2025

10.1126/science.adt0647